One- and two-photon phase-sensitive coherent-control scheme applied to photoionization microscopy of the hydrogen atom

P. Kalaitzis, D. Spasopoulos, and S. Cohen*

Atomic and Molecular Physics Laboratory, Physics Department, University of Ioannina, 45110 Ioannina, Greece

(Received 2 July 2019; published 16 October 2019)

Photoionization microscopy (PM) is an electron imaging method designed for the measurement of the outgoing flux of slow electrons produced by photoionization of atoms in the presence of an external uniform static electric field. The high resolution of PM allows the observation of spatial quantum interference structures which are directly related to the squared modulus of the excited electron's wave function. The PM's range of interest lies above the saddle-point energy, where continuum Stark states are degenerate with quasibound ones (resonances). A principal aim of PM is to provide access to the wave functions of the latter, which in hydrogen atoms ionize exclusively via tunneling (in contrast to the continuum states where the electron escapes freely above the potential barrier). In nonhydrogenic atoms, however, quasibound states are coupled with the continuum ones. Among other consequences, this leads to comparable resonant and continuum excitation strengths and the weakening or disappearance of the resonant manifestations from the recorded PM images. Here we examine theoretically the possibility of bypassing these difficulties by applying two-excitation-pathway interference techniques. For this first case-study we employ the hydrogen atom but we, nevertheless, simulate a nonhydrogenic situation by selecting hydrogenic Stark resonances whose excitation strengths are comparable to or even smaller than the continuum ones. Specifically, we consider the interaction of ground-state atoms with an $\omega/2\omega$ bichromatic laser field inducing one- and two-photon transitions to the final Stark states. It is shown that, under certain conditions and by appropriately adjusting the intensities of the two laser fields and their relative phase, the uncovering of resonant manifestations from PM images may indeed be achieved. Further work concerning theoretical extensions to complex atoms and possible experimental realizations are also discussed.

DOI: 10.1103/PhysRevA.100.043409

I. INTRODUCTION

Photoionization microscopy (PM) is an experimental technique designed for the measurement of the two-dimensional flux of slow (meV) electrons ejected during the photoionization of neutral atoms in the presence of a uniform static electric field. The electron current probability density is imaged by a position sensitive detector and the low energy of the liberated electrons allows for the observation of quantum interferences on the recorded images. In turn, as showed already by the first theoretical formulation of PM during the 1980s [1–3], these interference structures are directly related to the squared modulus of the electronic wave function.

The PM's theoretical framework is built upon the hydrogenic Stark effect and involves the so-called parabolic wave functions. The energy range of interest for PM studies lies just above the field-induced ionization threshold and it is characterized by coexisting (degenerate) continuum and quasibound Stark states (resonances). A primary aim of PM is to provide access to wave functions and interferences stemming from the resonances, the latter reflecting intrinsic properties of the atomic system under study. Experimental PM images unambiguously attributed to hydrogenic Stark resonances were recorded fairly recently [4] and fully verified the first age-old [2,3] as well as more recent [5–7] calculations. The resonant character imprinted on these images mainly consists of a significant size increase, along with the appearance of additional wave-function nodes with respect to the continuum images below and just above the resonance. For the experimentally employed single-photon excitation scheme out of an excited $n = 2$ hydrogenic state [4], the excitation strength of the resonances was found to be much stronger than that of the continua, leading to a comfortable identification of the aforementioned resonant manifestations. These manifestations, however, proved to be difficult to record in nonhydrogenic atoms. The latter are characterized by the emergence of short-range interactions induced by the penetration of the excited electron's wave function into the residual ionic core. As a consequence, each Stark state wave function outside the core is expressed as a mixture of regular and irregular wave functions of the corresponding hydrogenic parabolic state. Alternatively, nonhydrogenic Stark wave functions can be described as linear combinations of quasibound and continuum hydrogenic parabolic wave functions [8–10]. Then, a significant portion of an initially prepared resonant state population spreads out over several degenerate continua (autoionization), while resonant and continuum excitation amplitudes out of a given initial state become comparable. Thus, the image resonant features may be rather weak and hard to observe, and these difficulties grow with increasing ionic core size. This may explain why PM images of the heavy (atomic number $Z = 54$) Xe atom did not show resonant effects at all [11], despite the existence of theoretical predictions suggesting

*scohen@uoi.gr

that this would be possible under certain conditions in either Xe [12] or the alkali-metal atoms [8–10]. In fact, although somewhat less intense than in the hydrogenic data, resonant effects were indeed clearly observed in the PM images of the light nonhydrogenic atoms Li ($Z = 3$) [13,14] and He ($Z = 2$) [15]. In addition, they were apparent, albeit rather faint, even in the images of the medium-side Mg atom ($Z = 12$) [16].

Obviously, to efficiently overcome the difficulties encountered with nonhydrogenic atoms and thus extend the usefulness of PM, further efforts need to rely upon special excitation strategies and profit from the experience accumulated so far. For example, it is by now well known that for the resonant character to be visible the number of degenerate continua needs to be low. It is therefore advantageous to work immediately above the classical saddle-point energy [13,14]. Another example concerns the He PM experiment [15] where the resonant character was recorded near avoided crossings between pairs of interacting resonances [17], with the resonance of interest being effectively decoupled from the continua. Following the above reasoning, the purpose of the present work is to theoretically explore the efficiency of yet another approach that makes use of the interference between two excitation amplitudes. The latter amplitudes, describing the transfer of ground-state atoms to the final Stark states, are induced by means of a bichromatic laser field consisting of a fundamental frequency beam and one of its mutually coherent harmonics. Then, the manipulation of given "target" observables can be achieved by appropriately adjusting the intensities of the two beams and the relative phase between them.

Two-pathway interference and especially phase-sensitive coherent-control (PSCC) [18] techniques are successfully applied for about 20 years now (for extensive reviews, see Refs. [19–27]). The fundamental (ω) plus second harmonic (2ω) bichromatic laser field selected for the present study is the easiest to implement from the experimental point of view. Furthermore, this $\omega/2\omega$ frequency ratio is combined here with the most convenient one- and two-photon excitation schemes. The latter combination was employed in the past for the manipulation of photoelectron angular distributions (PADs) in atomic [28] or molecular [29] ionization, as well as photofragment angular distributions [30], photodissociation [31], and forward-backward asymmetries [32] in molecular systems. It was also found to be fruitful in controlling photocurrents in semiconductors [33]. More recently, PAD calculations were devoted to the interaction of hydrogen atoms with femtosecond VUV pulses in the region of an intermediate resonance and for either linearly [34] or circularly [35] polarized $\omega/2\omega$ laser fields. Even more recently, these calculations were extended to the Neon atom [36]. The only "weakness" of the scheme is that it does not allow control of total yields in free atoms and systems possessing inversion symmetry. It is therefore important to mention those one- and two-photon excitation PSCC variants that tackled the problem through the presence of a static electric field that mixes states of opposite parity. Indeed, total excitation/ionization yields was so far the observable of interest in either theoretical [37–39] or experimental [40,41] work along this direction. Instead, our present aim is to employ this PSCC scheme in an attempt to manipulate the electron current probability density (i.e., the PM images) and the observables related to it. This first application of the method is devoted to the relatively simpler case of the hydrogen atom and particularly to those hydrogenic Stark resonances whose excitation strengths are generally comparable to or smaller than the continuum ones. Contrary to conventional wisdom this is a situation that can be frequently met in hydrogen atom [7] and, in addition, it is typically encountered in nonhydrogenic atoms. We then apply suitable manipulation procedures that allow efficient uncovering of otherwise obscured resonant signatures from the PM images under this unfavourable circumstance.

The rest of the paper is organized as follows: In Sec. II we briefly describe the theory of the hydrogenic Stark effect in the continuum and we incorporate the $\omega/2\omega$, one-, and two-photon PSCC scheme into the PM framework. In Sec. III the optimum PSCC conditions are obtained for all relevant observables and then applied to a characteristic test-PM image which is analyzed in detail. Finally, in the conclusion Sec. IV possible directions of further work are discussed.

II. THEORY

A. The quantum mechanical Coulomb-Stark problem

Let us begin by briefly exposing the quantum mechanical treatment of a hydrogen atom in the presence of a homogeneous and static electric field $\mathbf{F} = F\mathbf{z}$. The corresponding Schrödinger equation is separable in semiparabolic coordinates [7,42,43], $\chi = [r + z]^{1/2} \geqslant 0$, $\upsilon = [r–z]^{1/2} \geqslant 0$, and $\varphi = \tan^{-1}(y/x)$, where $r = [x^2 + y^2 + z^2]^{1/2}$. The electron wave function is written as $\psi(\mathbf{r}) = [2\pi\chi\upsilon]^{-1/2} X(\chi) Y(\upsilon) e^{im\phi}$ (with $m = 0, \pm1, \pm2, \ldots$ being the magnetic quantum number) and separability leads to two differential equations which are written as (in a.u. $\hbar = e = m_e = 1$),

$$\left[-\frac{1}{2}\frac{d^2}{d\chi^2} + U_{X,\mathrm{eff}}(\chi) - 2Z_1\right] X(\chi) = 0,$$

$$U_{X,\mathrm{eff}}(\chi) = \frac{4m^2 - 1}{8\chi^2} + \frac{F\chi^4}{2} - E\chi^2, \tag{1a}$$

$$\left[-\frac{1}{2}\frac{d^2}{d\upsilon^2} + U_{Y,\mathrm{eff}}(\upsilon) - 2Z_2\right] Y(\upsilon) = 0,$$

$$U_{Y,\mathrm{eff}}(\upsilon) = \frac{4m^2 - 1}{8\upsilon^2} - \frac{F\upsilon^4}{2} - E\upsilon^2, \tag{1b}$$

with E denoting the energy and Z_1 and $Z_2 = Z–Z_1$ are separation constants linked via the nuclear charge Z (for hydrogen atom $Z = 1$). In the present work we are interested for the energy range above the classical saddle-point energy $E_{\mathrm{sp}}^{\mathrm{cl}} = -2[ZF]^{1/2}$ a.u. [44] and in what follows we employ, alternatively to E, the convenient reduced energy variable:

$$\varepsilon \equiv \frac{E}{|E_{\mathrm{sp}}^{\mathrm{cl}}|}. \tag{2}$$

The $\varepsilon \geqslant -1 (E \geqslant E_{\mathrm{sp}}^{\mathrm{cl}})$ range includes the field-free ionization limit $\varepsilon = E = 0$ and it is generally characterized by the electron escape to infinity. Therefore, the (scattering) problem is solved for given sets of fixed E, m, and F values. The form of the effective potential $U_{X,\mathrm{eff}}$ forces the bound electron

motion along the χ coordinate and the solution of Eq. (1a) leads to the quantization of Z_1 (and consequently of Z_2). The obtained $Z_1^{n_1,|m|}$ set is characterized by the quantum number $n_1 = 0, 1, 2\ldots$, counting the nodes of the corresponding (real) wave functions $X_{n_1,|m|}$ in the interval $(0, \infty)$.

Along the υ coordinate where the electron may escape to infinity the large-υ asymptotic form of wave function Y is [5,45]

$$\underset{\upsilon\to\infty}{Y} = C_Y \mathcal{M}(\upsilon)\sin[\theta(\upsilon)+\phi], \tag{3}$$

with $C_Y = [2/\pi]^{1/2}$ stemming from its energy normalization [5,44,46]. In Eq. (3) the function $\mathcal{M} > 0$ is the Milne function, obeying the Milne equation [47],

$$\left[\frac{d^2}{d\upsilon^2} + k^2\right]\mathcal{M} - \frac{1}{\mathcal{M}^3} = 0, \tag{4}$$

obtained by appropriately transforming Eq. (1b) [5,45]. In Eq. (4), $k^2(\upsilon) = 2[2Z_2^{n_1,|m|} – U_{Y,\text{eff}}(\upsilon)]$ is the squared wave-number function and it turns out that $\mathcal{M} \approx k^{-1/2}$ in the $\upsilon \to \infty$ limit. Finally, in Eq. (3),

$$\theta(\upsilon) = \int_{\upsilon_m}^{\upsilon} \frac{1}{\mathcal{M}^2(\upsilon')} d\upsilon', \tag{5}$$

and ϕ is a constant phase which depends on the lower integration limit υ_m.

Note that for $-1 \leqslant \varepsilon < 0$ the effective potential $U_{Y,\text{eff}}$ exhibits a barrier and each n_1 channel is associated to a threshold $E_{\text{thr}}^{n_1,|m|}$, given by the root of the equation $E + 2[Z_2^{n_1,|m|}(F,E)F]^{1/2} = 0$ [8,14,39,48]. For $E > E_{\text{thr}}^{n_1,|m|}$ the electron escapes over the barrier and its continuum state is characterized by the quantum number pair (n_1, m). When, however, $E < E_{\text{thr}}^{n_1,|m|}$ the electron may escape solely via tunneling through the barrier of $U_{Y,\text{eff}}$. In this case there are specific resonant values of $Z_2^{n_1,|m|}$ for which the amplitude of the wave function Y within the inner well of $U_{Y,\text{eff}}$ acquires large values. This fact reflects the entrapment of the electron at short distances and these, so-called, quasibound states (resonances) are characterized by an enlarged set of three quantum numbers (n_1, n_2, m), with n_2 being the number of nodes of Y within this inner well.

B. Phase-sensitive coherent control over the current probability density and related observables

Let us now consider the photo-excitation of the Stark states $\psi_{n_1,m}^{E,F}$ $(E \geqslant E_{\text{sp}}^{\text{cl}})$ out of a given initial state. The resulting outgoing flux of ionized electrons is described by the current probability density, $J_\upsilon(\chi,\phi) \propto i[\chi^2+\upsilon^2]^{-1/2}[\psi_{\text{out}}(\partial\psi_{\text{out}}^*/\partial\upsilon) - \psi_{\text{out}}^*(\partial\psi_{\text{out}}/\partial\upsilon)]$, along a paraboloid of constant υ. The calculation of $J_\upsilon(\chi,\phi)$ requires the knowledge of the υ-outgoing wave ψ_{out}, which is related to the $\psi_{n_1,m}^{E,F}$'s [3,5–7]. The relevant differential equation for ψ_{out} is derived from the time-dependent Schrödinger equation (TDSE), $i\partial\Psi/\partial t = [H(\mathbf{r}) + U(\mathbf{r},t)]\Psi$, where H is the Coulomb-Stark Hamiltonian and U the laser-atom interaction term. For the $\omega/2\omega$ PSCC scheme depicted in Fig. 1, the atoms interact with a fundamental frequency laser beam (ω) and its mutually coherent second harmonic (2ω). The two beams are assumed to be perfectly spatially overlapping. The

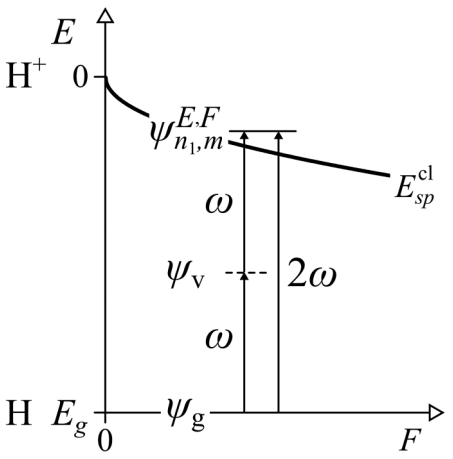

FIG. 1. Schematic energy-level diagram (not to scale) showing the presently examined $\omega/2\omega$, single-, and two-photon excitation PSCC scheme in the presence of a static homogeneous electric field of strength F. The two mutually coherent fields transfer ground-state hydrogen atoms (wave function ψ_g, energy E_g) to the final Stark states $\psi_{n_1,m}^{E,F}$, the latter located above the classical saddle-point energy $E_{\text{sp}}^{\text{cl}} = -2[ZF]^{1/2}$ a.u. and below the zero-field limit, $E = 0$. The two-photon transition proceeds via the virtual state ψ_v. For linear polarizations parallel to the direction of the static field, it holds that $m = 0$ for both the virtual and final states. The manipulation of given observables is achieved by adjusting the intensities of the two light beams and their relative phase.

total field is written as $\mathbf{E}_{\text{tot}}(t) = \boldsymbol{\varepsilon}_\omega\mathcal{E}_\omega(\exp[i(\omega t + \Phi_\omega)] + \text{c.c.}) + \boldsymbol{\varepsilon}_{2\omega}\mathcal{E}_{2\omega}(\exp[i(2\omega t + \Phi_{2\omega})] + \text{c.c.})$, where $\boldsymbol{\varepsilon}_\omega$ and $\boldsymbol{\varepsilon}_{2\omega}$ are linear polarization vectors, $\mathcal{E}_\omega$ and $\mathcal{E}_{2\omega}$ are real and time-independent amplitudes and Φ_ω and $\Phi_{2\omega}$ are fixed but controllable phases.

Working along the lines described in Ref. [49], we adopt an effective two-level model and Ψ is decomposed in two terms, one referring to the (initial) ground state ψ_g of energy E_g (and $m_g = 0$) and one to ψ_{out} of energy E. Thus, we write $\Psi(\mathbf{r},t) = \psi_g(\mathbf{r})e^{-iE_g t} + \psi_{\text{out}}(\mathbf{r})e^{-iEt}$, this form implying that the ground-state population is practically unaltered by either of the sufficiently weak laser fields and that ψ_{out} depends on the field amplitudes $\mathcal{E}_{\omega,2\omega}$. Further, the resonant condition is $2\omega = E - E_g$ and up to the lowest perturbative order the transition $\psi_g \to \psi_{\text{out}}$ is realized via either the absorption of a single photon from the $\mathcal{E}_{2\omega}$ field or by the absorption of two photons from the $\mathcal{E}_\omega$ field. Hence, the electric dipole interaction term may be written as $U(\mathbf{r},t) = U_{2\omega}^{(1)}(\mathbf{r},t) + U_\omega^{(2)}(\mathbf{r},t)$, where

$$U_{2\omega}^{(1)}(\mathbf{r},t) = \mathcal{E}_{2\omega}e^{-i(2\omega t+\Phi_{2\omega})}\boldsymbol{\varepsilon}_{2\omega}\cdot\mathbf{r} = \hat{T}_{2\omega}^{(1)}e^{-i2\omega t} \tag{6}$$

is responsible for single-photon transitions. Note that in Eq. (6) only the *resonant* absorption term ($\exp[-i2\omega t]$) is retained after the introduction of the rotating wave approximation [50], while the last equality defines the operator $\hat{T}_{2\omega}^{(1)}$. The resonant $U_\omega^{(2)}$ term may be put to the form [22,23,51,52],

$$U_\omega^{(2)}(\mathbf{r},t) = \mathcal{E}_\omega^2 e^{-i2(\omega t+\Phi_\omega)}\hat{D}^{(2)} = \hat{T}_\omega^{(2)}e^{-i2\omega t}, \tag{7}$$

where $\hat{D}^{(2)}$ is an effective two-photon electric dipole operator. There are no exactly- or near-resonant intermediate states in the vicinity of the first photon.

Strictly speaking, second-order ac Stark shifts induced by the $\mathcal{E}_\omega$ field should be also considered for the levels involved. These shifts, however, as estimated by ignoring the static field, turn out to be quite small. For example, the ground-state shift is given by $\delta E_g = -\alpha_d(\omega)\mathcal{E}_\omega^2/2$, where the dynamic dipole polarizability $\alpha_d(\omega)$ for $\omega \approx |E_g|/2$ is only slightly larger than its static value [53]. As for the near-threshold Rydberg levels, the so-called weak-field, high-frequency limit [54] implies that $\delta E = I_\omega/4\omega^2$ [55], where I_ω ($\propto\mathcal{E}_\omega^2$) is the fundamental beam intensity. By selecting I_ω to be sufficiently below the saturation intensity (say, $I_\omega \sim 10^9\,\mathrm{W/cm^2}$) we estimate an overall energy shift of the order of 10^{-7} a.u., i.e., smaller or comparable to the line-widths of long-pulse laser beams employed for such studies [4,15].

For the low field strengths of interest here the static electric field may indeed be neglected for the ground state. We nevertheless assume that ψ_g is an approximate eigenstate of $H(H\psi_g \approx E_g\psi_g)$. By inserting Ψ and U to TDSE and keeping terms linear in $\mathcal{E}_{2\omega}$ and quadratic in $\mathcal{E}_\omega$ (that is, by dropping the higher order $U(\mathbf{r},t)\psi_{\rm out}$ term [49]) one finally arrives at the so-called "Schrödinger equation with a source" [5,56] for $\psi_{\rm out}$ which is written as $(E-H)\psi_{\rm out} = (\hat{T}_{2\omega}^{(1)} + \hat{T}_\omega^{(2)})\psi_g$. Using the large-$\upsilon$ asymptotic, outgoing wave solution of this equation, the current probability density in the $\upsilon\to\infty$ limit is written as [5,7,9]

$$\underset{\upsilon\to\infty}{J_\upsilon}(\varphi,\chi) \propto \frac{1}{\chi\upsilon[\chi^2+\upsilon^2]^{1/2}} \times \left|\sum_{n_1,m} e^{i[\theta_{n_1,|m|}(\upsilon)+\phi_{n_1,|m|}]} d_{n_1,m} e^{im\varphi} X_{n_1,|m|}(\chi)\right|^2, \tag{8}$$

where

$$d_{n_1,m} = \left\langle \psi_{n_1,m}^{E,F} \middle| \hat{T}_{2\omega}^{(1)} + \hat{T}_\omega^{(2)} \middle| \psi_g \right\rangle \tag{9}$$

are transition matrix elements between ψ_g and the states $\psi_{n_1,m}^{E,F}$. The current probability density is imaged on an electron detector placed at $z_{\rm det} = -\upsilon_{\rm det}^2/2$ and whose plane is perpendicular to z axis. The radius ρ of electron impacts on the constant $\upsilon = \upsilon_{\rm det}$ paraboloid is given by $\rho = [x^2+y^2]^{1/2} = \chi\upsilon_{\rm det}$. For $\upsilon_{\rm det}\to\infty$ Eq. (8) is somewhat simplified since $[\chi^2+\upsilon_{\rm det}^2]^{1/2} \approx \upsilon_{\rm det}$.

The two-photon transitions may be described by single-photon ones, $\psi_{\rm v} \to \psi_{n_1,m}^{E,F}$, between the final states $\psi_{n_1,m}^{E,F}$ and a virtual state $\psi_{\rm v}$ [52,57,58,39,7] computed via the Dalgarno-Lewis method [59]. In other words, we may replace $\langle\psi_{n_1,m}^{E,F}|\hat{T}_\omega^{(2)}|\psi_g\rangle$ by $\langle\psi_{n_1,m}^{E,F}|\hat{T}_\omega^{(1)}|\psi_{\rm v}\rangle$, where, similar to Eq. (6), $\hat{T}_\omega^{(1)} = \mathcal{E}_\omega e^{-i\Phi_\omega}\boldsymbol{\varepsilon}_\omega\cdot\mathbf{r}$ is the single-photon dipole transition operator for the fundamental laser field. The static electric field is neglected also for the virtual state. Therefore, the relevant Dalgarno-Lewis equation is written as

$$\left[-\frac{1}{2}\nabla^2 - \frac{Z}{r} - E_{\rm v}\right]\psi_{\rm v} = -\hat{T}_\omega^{(1)}\psi_g, \tag{10}$$

with $E_{\rm v} = E_g + \omega = (E+E_g)/2$ [51,57,58].

For either the one- or two-photon excitation alone, if the magnitude of the matrix element of a resonance is much stronger than the matrix elements of the continuum channels, then the on-resonance current probability density will be dominated by this resonant state. This dominance is rather common in hydrogen atom [4,7], but as it will be shown shortly it cannot be generalized. It is interesting to note that the form of Eq. (8) remains apparently unchanged when dealing with nonhydrogenic atoms [8–10]. There, however, the aforementioned mixing between quasibound and continuum hydrogenic Stark states results in matrix elements differing significantly in modulus and phase with respect to the hydrogenic ones. Particularly, the modulus of resonant matrix elements usually becomes comparable to those of the continua while the resonant character may spread out over several n_1 channels [8–10,13,14,16].

For achieving PSCC over the population transferred to the final states the one-photon and two-photon transitions should necessarily excite the same m value [39]. Therefore, to eliminate any parasitic excitation we examine here the simplest possible case where the linear polarization vectors of both fields are parallel to the static electric field (π polarizations). Hence, $\boldsymbol{\varepsilon}_{2\omega}\cdot\mathbf{r} = \boldsymbol{\varepsilon}_\omega\cdot\mathbf{r} = z = (\chi^2-\upsilon^2)/2$ and because of the dipole selection rule $\Delta m = 0/per\text{-}photon$, only $m=0$ final states are populated. Then, by writing the virtual state in the form

$$\psi_{\rm v} = \mathcal{E}_\omega e^{-i\Phi_\omega}\tilde{\psi}_{\rm v} \tag{11}$$

(where $\tilde{\psi}_{\rm v}$ is also an $m=0$ state), Eq. (9) is written as

$$d_{n_1,m} = d_{n_1,0} \propto \mathcal{E}_{2\omega}D_{n_1,0}^{\pi(1)} + \mathcal{E}_\omega^2 e^{-i\Delta\Phi}D_{n_1,0}^{\pi(2)}, \tag{12}$$

where

$$D_{n_1,0}^{\pi(1)} = \left\langle\psi_{n_1,0}^{E,F}\middle|z\middle|\psi_g\right\rangle, \tag{13a}$$

$$D_{n_1,0}^{\pi(2)} = \left\langle\psi_{n_1,0}^{E,F}\middle|z\middle|\tilde{\psi}_{\rm v}\right\rangle \tag{13b}$$

are (real and independent of laser field amplitudes and phases) single- and two-photon transition matrix elements and

$$\Delta\Phi \equiv 2\Phi_\omega - \Phi_{2\omega}. \tag{14}$$

By angularly integrating Eq. (8), we may obtain the radial distribution

$$P(\rho) \propto \rho\int_0^{2\pi} J_{\upsilon_{\rm det}} d\phi, \tag{15}$$

which is proportional to the number of electron impacts within the $[\rho,\rho+d\rho]$ interval. For the present case where only $m=0$ states are included and $J_{\upsilon_{\rm det}}$ is independent of φ the integration is trivial and gives $P(\rho)\propto\rho J_{\upsilon_{\rm det}}(\rho)$. Finally, by integrating the current probability density over the whole surface of the $\upsilon_{\rm det}$ paraboloid we obtain the total electron signal, i.e., the total ionization rate $w_{\rm tot}$, which is written as [7]

$$w_{\rm tot} = \int J_{\upsilon_{\rm det}} dS \propto \sum_{n_1}\left|d_{n_1,0}\right|^2, \tag{16}$$

with dS the surface element of this paraboloid.

The calculation of initial, virtual and final state wave functions, as well as of the phases $\theta_{n_1,0}+\phi_{n_1,0}$ and the matrix

elements $D^{\pi(1)}_{n_1,0}$ and $D^{\pi(2)}_{n_1,0}$ was presented in detail elsewhere [7]. These computational procedures are followed here for obtaining the results concerning the manipulation and control of $w_{\rm tot}$, $P(\rho)$, and $J_{\upsilon_{\rm det}}$.

III. RESULTS AND DISCUSSION

A. General remarks

The application of PSCC under the presence of a static electric field offers a number of distinctive features and peculiarities. It is to be restated first that control over the total ionization rate $w_{\rm tot}$ via the simultaneous one- and two-photon atomic excitation necessitates the presence of the static field [34,37–39], which breaks the inversion symmetry characterizing field-free atoms. On the contrary, the field presence is not absolutely necessary for controlling observables related to the differential cross section, namely in our case the images $J_{\upsilon_{\rm det}}$ and radial distributions P.

Further, the PSCC efficiency for a given observable Ω is customarily assessed by the achieved contrast,

$$V^{\Omega} = \frac{\Omega^{+} - \Omega^{-}}{\frac{1}{2}(\Omega^{+} + \Omega^{-})}, \tag{17}$$

where Ω^{+} and Ω^{-} are the values of this observable for $\Delta\Phi = 0$ and $\Delta\Phi = \pi$, respectively. Note that the definition of Eq. (17) implies a maximum value of $|V^{\Omega}|$ equal to two. The optimum (maximum) absolute contrast value, $|V^{\Omega}_{\rm opt}|$, may be obtained as follows: By defining $\eta \equiv \mathcal{E}^2_{\omega}/\mathcal{E}_{2\omega}$ the matrix elements entering to $\Omega^{\pm}$ are written as $d_{n_1,0}(\Delta\Phi = 0) \propto D^{\pi(1)}_{n_1,0} + \eta D^{\pi(2)}_{n_1,0}$ and $d_{n_1,0}(\Delta\Phi = \pi) \propto D^{\pi(1)}_{n_1,0} - \eta D^{\pi(2)}_{n_1,0}$ [see Eq. (12)]. Then, the condition $dV^{\Omega}/d\eta = 0$ delivers a value of η for the given observable that leads to $V^{\Omega}_{\rm opt}$ when inserted to Eq. (17). It turns out that this optimum value of η implies always that $\Omega^{(1)} = \Omega^{(2)}$, the latter condition suggesting that contrast optimization is to be achieved when the individual single-photon and two-photon excitation recordings of that observable are equal [19,20,39]. However, obviously if either $\Omega^{(1)}$ or $\Omega^{(2)}$ is zero, then the observable cannot be controlled at all.

Let us apply the above considerations to the total excitation rate ($\Omega = w_{\rm tot}$). According to the above formulation the condition $w^{(1)} = w^{(2)}$ (emerging from the condition $dV^{w_{\rm tot}}/d\eta = 0$) translates to $\mathcal{E}^2_{2\omega}\sum_{n_1}\left(D^{\pi(1)}_{n_1,0}\right)^2 = \mathcal{E}^4_{\omega}\sum_{n_1}\left(D^{\pi(2)}_{n_1,0}\right)^2$ and can be realized by appropriate choices of the amplitudes $\mathcal{E}_{\omega}$ and $\mathcal{E}_{2\omega}$ of the two laser fields (or, equivalently, of their intensities). This leads to

$$V^{w_{\rm tot}}_{\rm opt} = 2\frac{\sum_{n_1}\left(D^{\pi(1)}_{n_1,0}D^{\pi(2)}_{n_1,0}\right)}{\left[\left(\sum_{n_1}\left(D^{\pi(1)}_{n_1,0}\right)^2\right)\left(\sum_{n_1}\left(D^{\pi(2)}_{n_1,0}\right)^2\right)\right]^{1/2}}. \tag{18}$$

Inspection of Eq. (18) reveals that, while the equality $w^{(1)} = w^{(2)}$ appears to be the only useful guideline for achieving the highest possible contrast, it does not guarantee that $|V^{w_{\rm tot}}_{\rm opt}|$ would be necessarily equal to the aforementioned maximum value of 2 [39]. This is due to the "collective" character of Eq. (18), which is expressed in terms of sums over all available n_1 channels. In fact, Eq. (12) suggests that it is possible to efficiently control each given individual channel (provided $D^{\pi(1)}_{n_1,0} \neq 0$ and $D^{\pi(2)}_{n_1,0} \neq 0$), but this, of course, does not imply that under the same conditions $w_{\rm tot}$ would be controlled with the same high efficiency (and vice versa). In accord to the above reasoning, for individual resonances below $E^{\rm cl}_{\rm sp}$ the presence of a single n_1 channel results indeed in $|V^{w_{\rm tot}}_{\rm opt}| = 2$. This is also approximately true just above $E^{\rm cl}_{\rm sp}$, where the number of n_1 channels and particularly the number of continua remains low. As energy increases further the number of channels grows and $|V^{w_{\rm tot}}_{\rm opt}|$ gradually drops to very low values [39]. Note finally that the variation of $V^{w_{\rm tot}}_{\rm opt}$ may also involve sign changes as a function of energy caused by changes of the relative sign of the one-photon and two-photon matrix elements which generally exhibit a drastic energy-dependence of magnitude and sign.

The relevant equalities $J^{(1)}_{\upsilon_{\rm det}} = J^{(2)}_{\upsilon_{\rm det}}$ and $P^{(1)} = P^{(2)}$ lead to a common optimum contrast expression,

$$V^{P}_{\rm opt}(\rho) = 2\frac{{\rm Re}\left[\left(\sum_{n_1} D^{\pi(1)}_{n_1,0}e^{i[\theta_{n_1,0}(\upsilon_{\rm det})+\phi_{n_1,0}]}X_{n_1,0}\right)\left(\sum_{n_1} D^{\pi(2)}_{n_1,0}e^{-i[\theta_{n_1,0}(\upsilon_{\rm det})+\phi_{n_1,0}]}X_{n_1,0}\right)\right]}{\left|\left(\sum_{n_1} D^{\pi(1)}_{n_1,0}e^{i[\theta_{n_1,0}(\upsilon_{\rm det})+\phi_{n_1,0}]}X_{n_1,0}\right)\left(\sum_{n_1} D^{\pi(2)}_{n_1,0}e^{i[\theta_{n_1,0}(\upsilon_{\rm det})+\phi_{n_1,0}]}X_{n_1,0}\right)\right|}, \tag{19}$$

which shares the same "collective" character with Eq. (18) for $w_{\rm tot}$, but clearly proposes a different optimization criterion with respect to it. Furthermore, Eq. (19) suggests that for fixed energy and F the magnitude and sign of the optimum contrast may vary with the radius ρ through the ρ-dependent wave functions $X_{n_1,0}$ (since $\rho \propto \chi$). In other words, each radial point of the image $J_{\upsilon_{\rm det}}$ or the radial distribution $P(\rho)$ may exhibit different $V^{P}_{\rm opt}$ values and, therefore, the uniform control of the full image or the full distribution cannot be guaranteed. These expectations are investigated below in some detail.

B. Uncovering the resonant character of photoionization microscopy images

The ability of PSCC to isolate the resonant characteristics of a given image will now be explored under conditions simulating a nonhydrogenic situation. To that purpose, we employ the example presented in Figs. 2 and 3. These graphs refer to a field strength of $F = 680\,{\rm V/cm}$ which falls within the typical range of strengths employed for PM studies and it was recently reported for either experimental (for the Mg atom) or theoretical (for the H atom) work [7,16]. Further, the selection of the energy range near $\varepsilon \approx -0.9$ serves two purposes. First, it ensures the presence of a fairly small but nonnegligible number of continua. Second, it includes the $(n_1, n_2, m) = (5, 26, 0)$ hydrogenic resonance for whom the ratio between resonant and continuum excitation strengths generally favors the continua. Specifically, consider the single-photon excitation rate $w^{(1)}$ given in Fig. 2(a) along with its individual, single n_1 channel, contributions for $0 \leqslant n_1 \leqslant 5$. All $n_1 > 5$ excitations are found to be negligibly small. The resonant ($n_1 = 5$) rate is stronger than any of the $n_1 = 0$–4 nonresonant ones. Nevertheless, at the spectral maximum of the resonance at

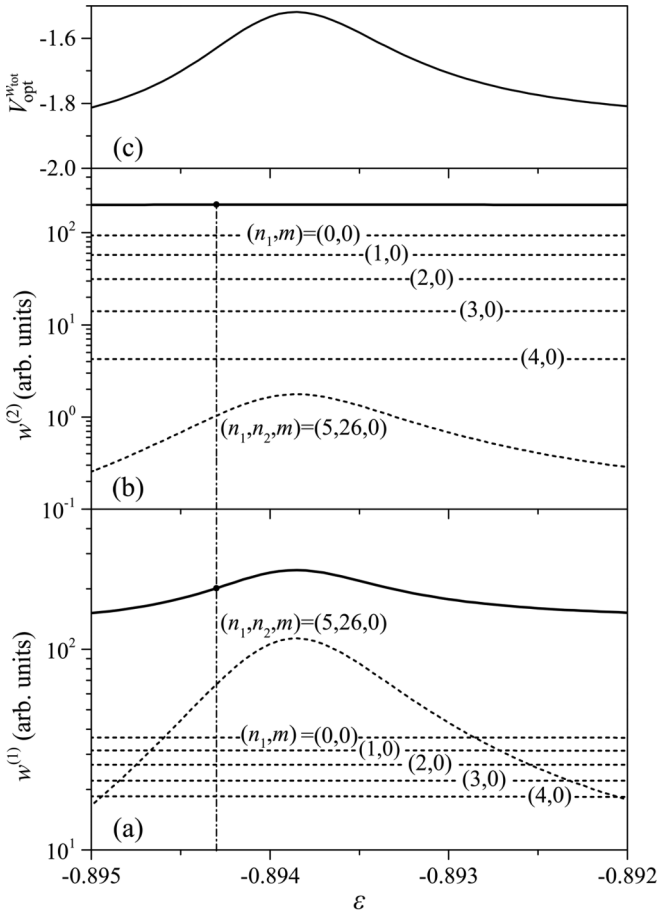

FIG. 2. (a) Calculated single-photon excitation/ionization of hydrogen atom out of its ground state with π-polarization ($m = 0$ final Stark states) in the presence of an electric field of strength $F = 680\,\mathrm{V/cm}$ and in the neighborhood of the $(n_1, n_2, m) = (5, 26, 0)$ Stark resonance (spectral maximum at reduced energy $\varepsilon_{\mathrm{res}} = -0.8939$). The bold solid line denotes the ionization rate $w^{(1)}$ and the dashed lines its individual n_1-contributions [see Eq. (16)]. (b) Same as in panel (a) but for the two-photon ionization rate $w^{(2)}$. The rate units are arbitrary but common in panels (a) and (b) and the equality $w^{(1)} = w^{(2)}$ holds for the reduced energy $\varepsilon = -0.8943 < \varepsilon_{\mathrm{res}}$, marked by the solid black points and the vertical dash-dotted line. This energy is employed for the calculations of Fig. 3. (c) The optimum contrast $V_{\mathrm{opt}}^{w_{\mathrm{tot}}}$ [Eq. (18)] as a function of ε. Note that $|V_{\mathrm{opt}}^{w_{\mathrm{tot}}}|$ is less than the maximum value of 2 over the whole range shown, while the negative value of $V_{\mathrm{opt}}^{w_{\mathrm{tot}}}$ implies an opposite relative sign between the one-photon and two-photon matrix elements $D_{n_1,0}^{\pi(1)}$ and $D_{n_1,0}^{\pi(2)}$, respectively.

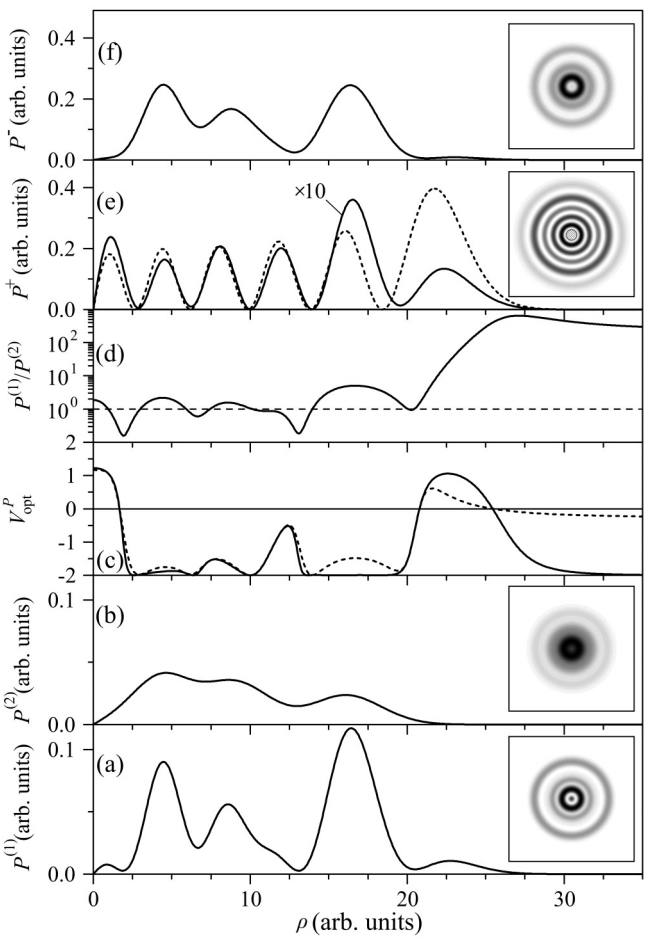

FIG. 3. (a) Calculated radial distribution $P^{(1)}(\rho)$ for single-photon ionization of hydrogen atom out of its ground state for $F = 680\,\mathrm{V/cm}$, $\varepsilon = -0.8943$, and π-polarized light ($m = 0$ final Stark states). (b) Same as in (a) but for the distribution $P^{(2)}(\rho)$ corresponding to two-photon ionization with π-polarized light. (c) Optimum contrast V_{opt}^{P} [Eq. (19)] as a function of ρ (solid line). (d) Ratio $P^{(1)}/P^{(2)}$ as a function of ρ (solid line). The horizontal dashed line shows the radii where the two distributions are chosen to be equal (as described in the text), so that they allow for the achievement of V_{opt}^{P}. Under this $P^{(1)}/P^{(2)}$ setting, the actually obtained contrast $V^{P}(\rho)$ is shown in panel (c) with a dashed line, the distribution $P^{+}(\rho)$ (multiplied by a factor of 10) for $\Delta\Phi = 0$ is shown in panel (e) and the distribution $P^{-}(\rho)$ for $\Delta\Phi = \pi$ is shown in (f). The insets of panels (a), (b), (e), and (f) show the corresponding images $J_{\upsilon_{\mathrm{det}}}^{(1)}$, $J_{\upsilon_{\mathrm{det}}}^{(2)}$, $J_{\upsilon_{\mathrm{det}}}^{+}$, and $J_{\upsilon_{\mathrm{det}}}^{-}$, respectively, where the gray scale is stretched from zero (white) to 100% (black) for each image except for (e) where the central maximum is cut at its 10% level (hatched area) for better visibility of the faint outer fringe. Additionally, in panel (e) also drawn with a dashed line is the squared wave function $X_{5,0}^{2}$, matched in magnitude with P^{+} at the maximum of the third bright fringe at $\rho \approx 8$ arb. units.

$\varepsilon_{\mathrm{res}} = -0.8939$ the nonresonant channels amount collectively to about half of the full magnitude of $w^{(1)}$ and their relative contribution grows significantly in the neighboring, slightly out of resonance, energy locations. As for the two-photon excitation given in Fig. 2(b), it favors the continua even more. The resonant contribution is about two orders of magnitude smaller than the stronger nonresonant ones. Consequently, the resonance is hardly visible in $w^{(2)}$. The essential differences between the single- and two-photon excitation spectra should not be surprising and they have already been pointed out in earlier work [7]. To verify former predictions [39] for PSCC over w_{tot}, Fig. 2(c) gives the optimum contrast $V_{\mathrm{opt}}^{w_{\mathrm{tot}}}$ as a function of ε, as emerged from the computed matrix elements $D_{n_1,0}^{\pi(1)}$ and $D_{n_1,0}^{\pi(2)}$. As a consequence of the existence of five nonnegligible channels, $|V_{\mathrm{opt}}^{w_{\mathrm{tot}}}|$ is not equal to 2 over the whole range around the resonance. In fact, for this specific resonance $|V_{\mathrm{opt}}^{w_{\mathrm{tot}}}|$ is found to be lower on-resonance than off-resonance.

Additionally, the negative sign of $V_{\rm opt}^{w_{\rm tot}}$ implies an opposite relative sign between single and two-photon matrix elements (which is indeed found to be the case for every n_1 value).

To mimic even more closely the nonhydrogenic case, calculations concerning PSCC over $J_{\upsilon_{\rm det}}$ and $P(\rho)$ are not performed at $\varepsilon_{\rm res}$ but at $\varepsilon = -0.8943 < \varepsilon_{\rm res}$, i.e., at the red side of the resonance [see Figs. 2(a) and 2(b)]. The observed behavior to be discussed below is visible in either the on-resonant or the off-resonant computations. For the latter, however, the uncovering of the resonant character is somewhat more spectacular. Figures 3(a) and 3(b) show the one- and two-photon distributions $P^{(1)}$ and $P^{(2)}$ and corresponding images $J_{\upsilon_{\rm det}}^{(1)}$ and $J_{\upsilon_{\rm det}}^{(2)}$, respectively. As it becomes obvious from Fig. 3(b), the aforementioned dominance of two-photon continuum excitation over the corresponding resonant one results to the complete absence of resonant features in $P^{(2)}$ and $J_{\upsilon_{\rm det}}^{(2)}$. The situation is not so dramatic for $P^{(1)}$ and $J_{\upsilon_{\rm det}}^{(1)}$ in Fig. 3(a). However, the comparable resonant and (collective) nonresonant contributions lead to important beating phenomena between them and, as a consequence, the resonant character of the image and radial distribution is partially lost. In particular, some of the dark fringes characterizing the $(n_1, n_2, m) = (5, 26, 0)$ resonance are obscured and the relative magnitudes of the maxima of $P^{(1)}$ do not correlate well with those of the squared wave function $X_{5,0}^2$. Further, the $V_{\rm opt}^P(\rho)$ curve emerging from Eq. (19) is given in Fig. 3(c). As it can be observed its sign is ρ-dependent. This reflects the combined effect of the opposite relative sign between the matrix elements $D_{n_1,0}^{\pi(1)}$ and $D_{n_1,0}^{\pi(2)}$, on the one hand, and of the ρ-dependence of the wave functions $X_{n_1,0}$ (changing sign between nodes), on the other. Specifically, $V_{\rm opt}^P(\rho)$ is positive as $\rho \to 0$ and within the $20.8 \leqslant \rho \leqslant 25.4$ arb. units radial interval, while negative everywhere else. This behavior implies that it is impossible to control the whole $P(\rho)$ distribution with the same efficiency, since, as is evident from Eq. (12), "subtraction" of (collective or individual n_1 channel) single- and two-photon contributions of opposite sign requires $\Delta\Phi = 0$, while their "addition" requires $\Delta\Phi = \pi$. The reverse conditions hold, of course, for contributions of the same sign. The above thinking guides the gross choice of the radial range where the optimum contrast condition $P^{(1)} = P^{(2)}$ will be imposed. For example, as Fig. 3(c) shows efficient control of the outer bright fringe of Fig. 3(a) whose maximum is located at $\rho \approx 23$ arb. units (and for which $V_{\rm opt}^P > 0$) is of little interest, because in practice it lies beyond the radial extend of $P^{(2)}$ [see Fig. 3(b)]. Furthermore, the largest part of the image around $2 \leqslant \rho \leqslant 20$ arb. units (for which $V_{\rm opt}^P < 0$) will then be totally uncontrolled. In fact, this last radial range appears to be the most interesting one because it includes the majority of nodes of the resonant contribution $X_{5,0}$. Clearly, then, under this choice the most efficient uncovering of resonant image features is to be achieved by P^+ ($\Delta\Phi = 0$ leading to "subtraction"). The next step toward this goal is the fine selection of the radius (or radii) where the condition $P^{(1)} = P^{(2)}$ will be applied. By denoting this radius as $\rho_{\rm o}$, its fine choice is based in the present work on the maximization of the overlap integral,

$$\mathrm{Ov}(\rho_{\rm o}) \equiv \int_0^\infty \tilde{P}^+(\rho_{\rm o}, \rho) X_{5,0}^2(\rho) d\rho, \tag{20}$$

where the wave function $X_{5,0}$ is normalized according to

$$\int_0^\infty X_{5,0}^2(\rho) d\rho = 1, \tag{21}$$

and similarly the "normalization condition"

$$\int_0^\infty \tilde{P}^+(\rho_{\rm o}, \rho) d\rho = 1. \tag{22}$$

is applied to the distribution $\tilde{P}^+(\rho_{\rm o}, \rho) = c(\rho_{\rm o}) P^+(\rho_{\rm o}, \rho)$, effectively determining the "normalization constant" $c(\rho_{\rm o})$.

The above optimization procedure led to the value $\rho_{\rm o} \approx 10$ arb. units, i.e., close to the third node of $X_{5,0}$. This result is drawn by a dashed horizontal line in Fig. 3(d) showing the selected ratio $P^{(1)}/P^{(2)}$ (equal to 1 at $\rho_{\rm o}$ as well as at $\approx$1, $\approx$3, $\approx$6, 14 arb. units etc., i.e., always near the nodes of $X_{5,0}$). It is also interesting to compare the optimum $V_{\rm opt}^P(\rho)$ curve with the actually achieved $V^P(\rho_{\rm o}, \rho)$, the latter given in Fig. 3(c) with a dashed line. However, the PSCC efficiency can be fully appreciated by inspecting Figs. 3(e) and 3(f). In fact, the comparison given in Fig. 3(e) between the optimized distribution P^+ and the "target" squared wave function $X_{5,0}^2$ reveals a fairly close resemblance between them over all radii but the last two lobes and especially the more distant one within the $20 \leqslant \rho \leqslant 27$ arb. units radial interval. Considering the discussion above and the specificities of the examined case, this is an expected result. Finally, the distribution P^-, computed under the same conditions but for $\Delta\Phi = \pi$, is clearly dominated by the continuum contributions, albeit with different relative n_1-weights with respect to those of the distribution $P^{(2)}$ of Fig. 3(b).

IV. OUTLOOK AND CONCLUDING REMARKS

We have presented a theoretical study devoted to an excitation strategy aiming to unmask the resonant signatures from photoionization microscopy images when the excitation strength of the Stark resonant state of interest is dominated by the corresponding continuum ones. The strategy involves an $\omega/2\omega$, one-, and two-photon excitation phase-sensitive coherent-control scheme and has been applied to images of near-saddle-point hydrogenic resonances satisfying the above unfavorable excitation criterion and thus probing a nonhydrogenic situation. Using a typical example, it has been shown that, by following an appropriately adapted protocol for the choice of the two laser-field amplitudes and relative phase, the dominance of the resonant characteristics over the image can indeed be achieved.

In general, a low number of contributing n_1 channels has been found to be quite beneficial and to allow for manipulation and efficient control of individual channels. Depending on the specificities of the given static-field strength, energy range and target resonance, further favourable conditions and protocol refinements may apply, concerning, for example, the (possibly reversed) relative sign between the resonant and continuum excitation matrix elements. Furthermore, control and phase manipulation is generally possible even when the number of n_1 channels is high, despite the fact that, as earlier work [39] and present tests have shown, it is rather unlikely to obtain high overall modulation contrasts in those cases. The scope

of phase manipulation, however, is not necessarily exhausted to the achievement of high contrasts. Therefore, the method might also be useful in other, presently unthought-of, applications making use of the introduction of an experimentally controllable phase to the current probability density (differential ionization cross section) which, in our case, is already dominated by intense quantum interference effects.

Evidently, the quite promising results of the present work call for its extension to nonhydrogenic atoms. Notably, this extension will bring n_1 channel mixing into play. As already mentioned, of particular importance is the detrimental role of the mixing between closed and open channels (resonances and continua, respectively) and the resulting spread of the resonant state population over several continua. Neither the present nor any other two-excitation-pathway control scheme can affect the n_1 channel coupling. Qualitatively, however, one may expect that it would be feasible to recover the resonant signatures as long as they are clearly manifested in at least one channel, despite the fact that this channel may perhaps be rather weakly excited. Moreover, another, apparently even more interesting, possibility would be to additionally exploit the mixing among closed channels, namely to examine the application of phase control in the vicinity of avoided crossings between interacting resonances. Then, even more fruitful results are to be expected from the combination of the facts that (i) for an appropriate static-field strength one of these resonances frequently decouples from the continua thus making the recording of resonant images easier [15] and (ii) the application of the proposed phase control scheme was predicted to significantly reduce the continuum excitation under appropriate selection of the parameters of the two laser beams [39]. We are currently working toward these directions, theoretically as well as experimentally.

ACKNOWLEDGMENTS

The authors thank S. Danakas, C. Bordas, F. Lépine, and K. Ferentinou for fruitful discussions. The research (MIS: 5005247) is implemented through the Operational Program "Human Resources Development, Education and Lifelong Learning" and is co-financed by the European Union (European Social Fund) and Greek national funds.

[1] I. I. Fabrikant, Z. Eksp. Teor. Fiz. **79**, 2070 (1980) [Sov. Phys. JETP **52**, 1045 (1980)].
[2] Yu. N. Demkov, V. D. Kondratovich, and V. N. Ostrovsky, Pis'ma Z. Eksp. Teor. Fiz. **34**, 425 (1981) [JETP Lett. **34**, 403 (1981)].
[3] V. D. Kondratovich and V. N. Ostrovsky, J. Phys. B **17**, 1981 (1984); **17**, 2011 (1984); **23**, 21 (1990); **23**, 3785 (1990).
[4] A. S. Stodolna, A. Rouzée, F. Lépine, S. Cohen, F. Robicheaux, A. Gijsbertsen, J. H. Jungmann, C. Bordas, and M. J. J. Vrakking, Phys. Rev. Lett. **110**, 213001 (2013).
[5] L. B. Zhao and J. B. Delos, Phys. Rev. A **81**, 053418 (2010).
[6] L. B. Zhao, D. H. Xiao, and I. I. Fabrikant, Phys. Rev. A **91**, 043405 (2015).
[7] P. Kalaitzis, S. Danakas, F. Lépine, C. Bordas, and S. Cohen, Phys. Rev. A **97**, 053412 (2018).
[8] D. A. Harmin, Phys. Rev. A **26**, 2656 (1982); **24**, 2491 (1981).
[9] P. Giannakeas, F. Robicheaux, and C. H. Greene, Phys. Rev. A **91**, 043424 (2015).
[10] L. B. Zhao, I. I. Fabrikant, J. B. Delos, F. Lépine, S. Cohen, and C. Bordas, Phys. Rev. A **85**, 053421 (2012); L. B. Zhao, I. I. Fabrikant, M. L. Du, C. Bordas, and L. B. Zhao, Europhys. Lett. **109**, 23002 (2015).
[11] C. Nicole, H. L. Offerhaus, M. J. J. Vrakking, F. Lépine, and C. Bordas, Phys. Rev. Lett. **88**, 133001 (2002); C. Bordas, F. Lépine, C. Nicole, and M. J. J. Vrakking, Phys. Rev. A **68**, 012709 (2003); F. Lépine, C. Bordas, C. Nicole, and M. J. J. Vrakking, *ibid.* **70**, 033417 (2004).
[12] F. Texier, Phys. Rev. A **71**, 013403 (2005).
[13] S. Cohen, M. M. Harb, A. Ollagnier, F. Robicheaux, M. J. J. Vrakking, T. Barillot, F. Lépine, and C. Bordas, Phys. Rev. Lett. **110**, 183001 (2013).
[14] S. Cohen, M. M. Harb, A. Ollagnier, F. Robicheaux, M. J. J. Vrakking, T. Barillot, F. Lépine, and C. Bordas, Phys. Rev. A **94**, 013414 (2016).
[15] A. S. Stodolna, F. Lépine, T. Bergeman, F. Robicheaux, A. Gijsbertsen, J. H. Jungmann, C. Bordas, and M. J. J. Vrakking, Phys. Rev. Lett. **113**, 103002 (2014).
[16] P. Kalaitzis, S. Danakas, C. Bordas, and S. Cohen, Phys. Rev. A **99**, 023428 (2019).
[17] M. L. Zimmerman, M. G. Littman, M. M. Kash, and D. Kleppner, Phys. Rev. A **20**, 2251 (1979); S. Feneuille, S. Liberman, E. Luc-Koenig, J. Pinard, and A. Taleb, J. Phys. B **15**, 1205 (1982); J. Y. Liu, P. McNicholl, D. A. Harmin, J. Ivri, T. Bergeman, and H. J. Metcalf, Phys. Rev. Lett. **55**, 189 (1985); P. McNicholl, T. Bergeman, and H. J. Metcalf, Phys. Rev. A **37**, 3302 (1988).
[18] M. Shapiro, J. W. Hepburn, and P. Brumer, Chem. Phys. Lett. **149**, 451 (1988).
[19] M. Shapiro and P. Brumer, in *Advances in Atomic, Molecular, and Optical Physics*, edited by B. Bederson and H. Walther, Vol. 42 (Academic Press, San Diego, 2000), p. 287.
[20] E. Ehlotzky, Phys. Rep. **345**, 175 (2001).
[21] P. Brumer and M. Shapiro, *Principles of the Quantum Control of Molecular Processes* (Wiley-VCH, Berlin, 2003).
[22] M. Shapiro and P. Brumer, Rep. Prog. Phys. **66**, 859 (2003).
[23] M. Shapiro and P. Brumer, Phys. Rep. **425**, 195 (2006).
[24] V. A. Astapenko, Quant. Electron. **36**, 1131 (2006).
[25] C. Brif, R. Chakrabarti, and H. Rabitz, New J. Phys. **12**, 075008 (2010).
[26] H. Ohmura in *Advances in Multiphoton Processes and Spectroscopy*, edited by S. H. Lin, A. A. Villaeys, and Y. Fugimura (Word Scientific, Singapore, 2014), pp. 55–103.
[27] T. Scholak and P. Brumer, Adv. Chem. Phys. **62**, 39 (2017).
[28] N. B. Baranova, I. B. Beterov, B. Y. Zel'dovich, I. I. Ryabtsev, A. N. Chudinov, and A. A. Shul'ginov, JETP Lett. **55**, 439 (1992); Y. Y. Yin, C. Chen, D. S. Elliott, and A. V. Smith, Phys. Rev. Lett. **69**, 2353 (1992); Z. M. Wang and D. S. Elliott, *ibid.* **87**, 173001 (2001); R. Yamazaki, and D. S. Elliott, *ibid.* **98**, 053001 (2007).

[29] Y. Y. Yin, D. S. Elliott, R. Shehadeh, and E. R. Grant, Chem. Phys. Lett. **241**, 591 (1995).
[30] H. Ohmura, T. Nakanaga, and M. Tachiya, Phys. Rev. Lett. **92**, 113002 (2004).
[31] B. Sheehy, B. Walker, and L. F. DiMauro, Phys. Rev. Lett. **74**, 4799 (1995); H. Omura, T. Nakanaga, H. Arakawa, and M. Tachiya, Chem. Phys. Lett. **363**, 559 (2002).
[32] H. Ohmura, F. Ito, and M. Tachiya, Phys. Rev. A **74**, 043410 (2006).
[33] N. B. Baranova, A. N. Chudinov, and B. Y. Zel'dovich, Opt. Commun. **79**, 116 (1990); E. Dupont, P. B. Corkum, H. C. Liu, M. Buchanan, and Z. R. Wasilewski, Phys. Rev. Lett. **74**, 3596 (1995); J. K. Wahlstrand, H. Zhang, S. B. Choi, S. Kannan, D. S. Dessau, J. E. Sipe, and S. T. Cundiff, *ibid.* **106**, 247404 (2011).
[34] A. N. Grum-Grzhimailo, E. V. Gryzlova, E. I. Staroselskaya, J. Venzke, and K. Bartschat, Phys. Rev. A **91**, 063418 (2015).
[35] N. Douguet, A. N. Grum-Grzhimailo, E. V. Gryzlova, E. I. Staroselskaya, J. Venzke, and K. Bartschat, Phys. Rev. A **93**, 033402 (2016).
[36] E. V. Gryzlova, A. N. Grum-Grzhimailo, E. I. Staroselskaya, N. Douguet, and K. Bartschat, Phys. Rev. A **97**, 013420 (2018).
[37] N. L. Manakov, V. D. Ovsiannikov, and A. F. Starace, Phys. Rev. Lett. **82**, 4791 (1999).
[38] V. A. Astapenko, Quant. Electron. **35**, 541 (2005).
[39] S. Cohen, J. Phys. B **44**, 205402 (2011).
[40] M. Gunawardena and D. S. Elliott, Phys. Rev. Lett. **98**, 043001 (2007); Phys. Rev. A **76**, 033412 (2007).
[41] A. Bolovinos, S. Cohen, and I. Liontos, Phys. Rev. A **77**, 023413 (2008).
[42] R. J. Damburg and V. V. Kolosov, J. Phys. B **9**, 3149 (1976).
[43] H. Cartarius, J. Main, T. Losch, and G. Wunner, Phys. Rev. A **81**, 063414 (2010).
[44] T. F. Gallagher, *Rydberg Atoms* (Cambridge University Press, Cambridge, 1994), and references therein.
[45] A. Alijah, J. T. Broad, J. Hinze, and A. Alijah, J. Phys. B **25**, 5043 (1992).
[46] H. A. Bethe and E. E. Salpeter, *Quantum Mechanics of One and Two-Electron Atoms* (Springer, Berlin, 1957), and references therein.
[47] W. E. Milne, Phys. Rev. **35**, 863 (1930).
[48] E. Luc-Koenig and A. Bachelier, J. Phys. B **13**, 1743 (1980); **13**, 1769 (1980).
[49] T. Topçu and F. Robicheaux, J. Phys. B **40**, 1925 (2007).
[50] R. Loudon, *The Quantum Theory of Light*, 2nd ed. (Clarendon, Oxford University Press, New York, 1983).
[51] T. Nakajima and P. Lambropoulos, Phys. Rev. A **50**, 595 (1994).
[52] B. Gao and A. F. Starace, Phys. Rev. A **39**, 4550 (1989).
[53] S. Cohen and S. Themelis, J. Chem. Phys. **124**, 134106 (2006).
[54] N. B. Delone and V. P. Krainov, Phys. Usp. **42**, 669 (1999).
[55] N. J. van Druten, R. Trainham, and H. G. Muller, Phys. Rev. A **50**, 1593 (1994).
[56] C. Bracher, T. Kramer, and M. Kleber, Phys. Rev. A **67**, 043601 (2003); T. Kramer, C. Bracher, and M. Kleber, J. Phys. A: Math. Gen. **35**, 8361 (2002).
[57] E. S. Toma and H. G. Muller, J. Phys. B **35**, 3435 (2002).
[58] R. B. Thayyullathil and K. J. Prasanna, Phys. Rev. A **49**, 2432 (1994); R. B. Thayyullathil, R. Radhakrishnan, and M. Seema, J. Phys. A: Math. Gen. **36**, 8473 (2003).
[59] A. Dalgarno and J. T. Lewis, Proc. R. Soc. London, Ser. A **233**, 70 (1955).